






Evidence for Bootstrap Percolation Dynamics in a Photoinduced Phase Transition

Tyler Carbin,^{1,*} Xinshu Zhang¹,,¹ Adrian B. Culver^{1,2},,^{1,2} Hengdi Zhao,³ Alfred Zong^{4,5},,^{4,5} Rishi Acharya,¹ Cecilia J. Abbamonte¹,,¹ Rahul Roy,^{1,2} Gang Cao,³ and Anshul Kogar^{1,†}

¹*Department of Physics and Astronomy, University of California Los Angeles, Los Angeles, California 90095-1547, USA*

²*Mani L. Bhaumik Institute for Theoretical Physics, Department of Physics and Astronomy, University of California Los Angeles, Los Angeles, California 90095, USA*

³*Department of Physics, University of Colorado at Boulder, Boulder, Colorado 80309, USA*

⁴*Department of Chemistry, University of California at Berkeley, Berkeley, California, 94720, USA*

⁵*Materials Sciences Division, Lawrence Berkeley National Laboratory, Berkeley, California, 94720, USA*

 (Received 21 October 2022; revised 27 January 2023; accepted 30 March 2023; published 5 May 2023)

Upon intense femtosecond photoexcitation, a many-body system can undergo a phase transition through a nonequilibrium route, but understanding these pathways remains an outstanding challenge. Here, we use time-resolved second harmonic generation to investigate a photoinduced phase transition in $\text{Ca}_3\text{Ru}_2\text{O}_7$ and show that mesoscale inhomogeneity profoundly influences the transition dynamics. We observe a marked slowing down of the characteristic time τ that quantifies the transition between two structures. τ evolves nonmonotonically as a function of photoexcitation fluence, rising from below 200 fs to ~ 1.4 ps, then falling again to below 200 fs. To account for the observed behavior, we perform a bootstrap percolation simulation that demonstrates how local structural interactions govern the transition kinetics. Our work highlights the importance of percolating mesoscale inhomogeneity in the dynamics of photoinduced phase transitions and provides a model that may be useful for understanding such transitions more broadly.

DOI: [10.1103/PhysRevLett.130.186902](https://doi.org/10.1103/PhysRevLett.130.186902)

In a photoinduced phase transition (PIPT), a qualitative and macroscopic change to the behavior of a many-body system occurs following intense femtosecond photoexcitation. PIPTs are inherently different from equilibrium transitions because they typically proceed through a far from equilibrium, nonthermal pathway where time becomes a fundamental variable. Tracking the temporal evolution of the spatially averaged response functions is crucial to understanding the spectacular behaviors instigated by photoexcitation in solids, such as the appearance of transient order and metastability of hidden states [1–6]. However, order often evolves in a spatially nonuniform manner in many PIPTs; a major recurring theme is the presence of electronic and crystallographic inhomogeneity on the nano- to microscale [7–25].

Experimentally capturing the *dynamics* of mesoscale structures has proven difficult. However, inhomogeneous textures have been observed in materials exhibiting long-lived metastability following photoexcitation. In the metastable “hidden” states of both 1T-TaS₂ [1,26,27] and strained La_{2/3}Ca_{1/3}MnO₃ [2,28], quasistatic textures were observed using real-space scanning probe techniques. But, such experimental approaches are currently unfeasible for observing inhomogeneity that evolves on the short time-scales characteristic of many PIPTs. A notable exception is the insulator-metal PIPT in VO₂, which was found to exhibit similar transient textures determined by grain boundaries or preexisting domains following each applied

laser pulse [13,14,16]. To understand the effects of the dynamic inhomogeneity, our approach here is to quantify its aggregate effects on macroscopic observables and correlate the observations with a time-dependent statistical model.

To accomplish this goal, we employ time-resolved second harmonic generation (SHG) to investigate a PIPT in a prototypical correlated material, $\text{Ca}_3\text{Ru}_2\text{O}_7$ (CRO), in which photoinduced inhomogeneity is expected to occur (see below). By relating the experimental observations to simulation results, we provide strong evidence that structural percolation, mediated by lattice strain, governs the transition kinetics. Specifically, we show that the photoinduced dynamics are consistent with bootstrap percolation, a particular cellular automata model that lacks detailed balance.

$\text{Ca}_3\text{Ru}_2\text{O}_7$ (CRO) is the $n = 2$ compound in the Ruddlesden-Popper series $\text{Ca}_{n+1}\text{Ru}_n\text{O}_{3n+1}$ [29]. The crystal is distorted from the typical $I4/mmm$ structure due to rotation and tilts of the oxygen octahedra around the (001) axis and (110) axis, respectively [Fig. 1(b)]. At all temperatures, its crystallographic space group is $Bb2_1m$ (No. 36), with point group C_{2v} . As the temperature is reduced below the Néel temperature, $T_N = 56$ K, CRO undergoes a continuous phase transition to an antiferromagnetic state in which the Ru spins are aligned ferromagnetically along the $\pm a$ axis within each bilayer and antiferromagnetically between bilayers [30]. Of primary interest here is the discontinuous metal-insulator transition at $T_{MI} = 48$ K.

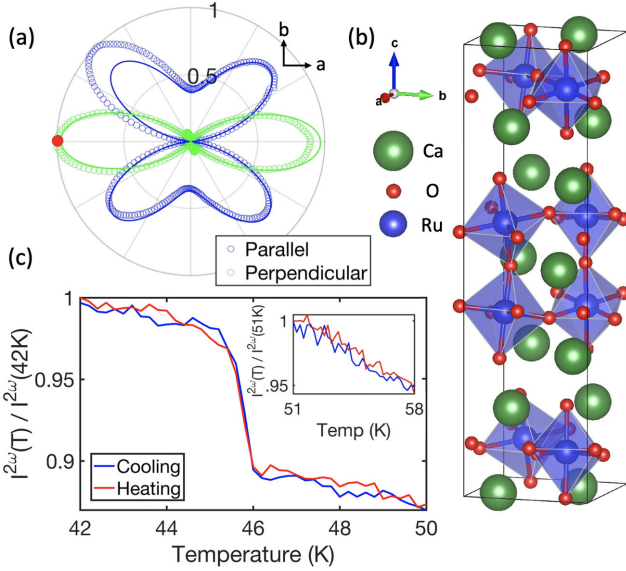


FIG. 1. (a) Measured RA-SHG patterns at 52 K with incident and outgoing polarizers in parallel and perpendicular geometry. Simultaneous fits to both channels are obtained using a susceptibility tensor constrained by the C_{2v} point group (solid lines). The data are normalized to a maximum in the perpendicular channel. The a and b crystallographic axes are indicated with black arrows. (b) Schematic of the low-temperature crystal structure. (c) Temperature dependence of the SHG intensity $I^{2\omega}$ at a polarization angle indicated by the red dot in (a). In this geometry, $I^{2\omega} \propto |\chi_{baa}^{ED}|^2$. The red (blue) curve corresponds to heating (cooling). Inset: normalized $I^{2\omega} \propto |\chi_{baa}^{ED}|^2$ across T_N .

In samples grown by the floating zone method, the low-temperature state is semimetallic [31–33], but in the flux-grown samples used here, this state is truly insulating [34]. This electronic transition is accompanied by a rotation of the spins from the $\pm a$ axis to the $\pm b$ axis [30,35] and a structural transition without a change in crystallographic symmetry. Through the transition, the c axis contracts by $\sim 0.1\%$ and the a and b axis lattice parameters expand by $\sim 0.07\%$ [29]. The structural change leads to a compression of the oxygen octahedra and further breaks the degeneracy between the Ru d_{xy} and the $d_{xz/yz}$ orbitals; it is therefore thought to be a vital component of the insulator-metal transition by promoting an orbital polarization [35–39].

To probe the dynamics of the phase transition, we perform time-resolved SHG, a technique that can monitor the symmetry of CRO in its various phases [40]. These measurements were performed in a reflection geometry, using 180 fs laser pulses with a 5 kHz repetition rate. We collected data in two configurations—one with parallel and one with perpendicular incident and outgoing light polarization. The probe beam was centered at 900 nm (1.38 eV) and was shone normal to the ab plane with a 40 μm spot size. The pump beam was centered at 1030 nm (1.20 eV) and was incident at 15° to the surface normal with a 200 μm spot size. When the system is pumped with the laser pulse,

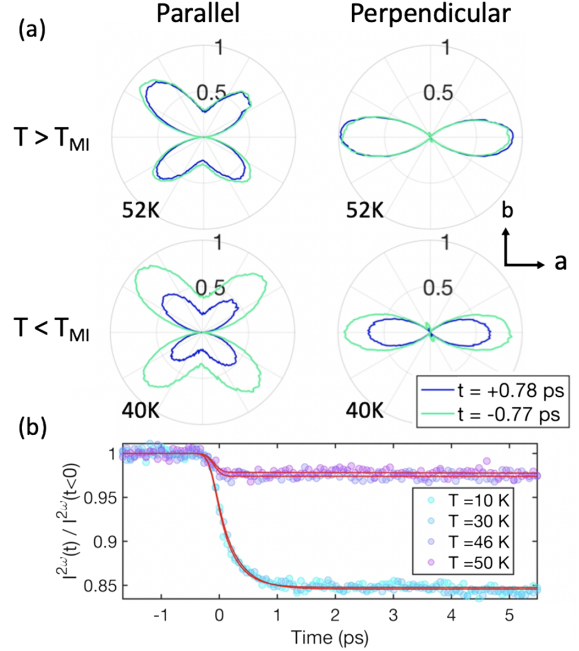


FIG. 2. Temperature-dependent SHG response to the 1030 nm pump pulse. (a) Rotational anisotropy patterns measured before ($t < 0$) and after ($t > 0$) a 0.28 mJ/cm^2 pump pulse both above and below T_{MI} . The pulse induces a large drop in SHG intensity when applied below T_{MI} and has little effect above T_{MI} . (b) Time traces of the normalized SHG intensity $I^{2\omega} \propto |\chi_{baa}^{ED}|^2$ at several temperatures with a 0.86 mJ/cm^2 pulse. Red lines are fits to Eq. (1). Traces at additional temperatures are excluded here for clarity and are presented in Supplemental Material [42].

the excited electrons remain within the t_{2g} manifold of the Ru^{4+} atoms (the crystal field splitting to the e_g levels is $\sim 2 \text{ eV}$) [41].

In the equilibrium state, the leading-order electric-dipole (ED) SHG contribution is allowed in CRO due to broken inversion symmetry (Fig. 1). At all temperatures, we obtain a good simultaneous fit to the parallel and perpendicular polarization configurations of the rotational anisotropy (RA) pattern with the ED contribution of the known point group symmetry C_{2v} [42] [Fig. 1(a)]. In Fig. 1(c), we show the temperature dependence of the SHG intensity $I^{2\omega}$ arising from the tensor element χ_{baa}^{ED} [red dot in Fig. 1(a)] across the insulator-metal transition. Although there is no temperature-induced change in symmetry of the RA pattern across the insulator-metal transition (Fig. 2(a)), the intensity exhibits a pronounced jump. (The offset between the reported value for $T_{MI} = 48 \text{ K}$ and the observed jump around 46 K arises due to laser heating) [42]. No thermal hysteresis is measured, and no features are observed at T_N [Fig. 1(c) inset].

Because the crystal, electronic and magnetic structure all change at T_{MI} , the cause of the observed jump in $I^{2\omega}$ is not immediately clear. A previous study reports a similar increase in $I^{2\omega}$ for pure CRO, but observes no such feature

in the Fe-doped compound $\text{Ca}_3\text{Ru}_{1.95}\text{Fe}_{0.05}\text{O}_7$ [58]. This difference is striking because, similar to pure CRO, the latter compound undergoes a transition in which the spins reorient from pointing along the $\pm a$ axis to the $\pm b$ axis and a concomitant metal-insulator transition. However, unlike in pure CRO, this transition is not accompanied by a large structural change [37,59]. We therefore conclude that the increase in $I^{2\omega}$ is indicative of the structural change [note that this is consistent with no features being observed at T_N Fig. 1(c)]. To corroborate the connection between crystal structure and $I^{2\omega}$, in Supplemental Material we use a Landau theory approach to show that a first-order transition with a symmetry-preserving order parameter can give rise to a jump in $I^{2\omega}$ [42].

We now study the PIPT instigated by intense femto-second laser pulses. Figure 2(a) shows the change in the RA-SHG pattern above and below T_{MI} after the arrival of a 0.28 mJ/cm^2 pump pulse. Below T_{MI} , there is a clear drop in intensity following the pulse, while the pattern above T_{MI} is minimally affected. As in the thermal transition, the symmetry is unchanged. Figure 2(b) shows the evolution of $I^{2\omega} \propto |\chi_{baa}^{ED}|^2$ after photoexcitation at several temperatures. These curves demonstrate that the decrease in intensity is stable for $\gg 5 \text{ ps}$. The magnitude of the drop in $I^{2\omega}$ is roughly constant for various temperatures below T_{MI} , but is markedly smaller in the high-temperature phase. (Here, the measured T_{MI} is between 44–45 K due to laser heating from both pump and probe pulses.) It should be noted that the intensity of the second harmonic $I^{2\omega}$ varies across the sample surface (the ab plane) due to the nonuniform distribution of 180° polar domains, as discussed more thoroughly in Refs. [42,60]. However, the photoinduced changes are associated only with the phase transition [42].

To understand the kinetics of the PIPT, we measure SHG time traces in the low temperature state for various pump fluences [Fig. 3(a)]. We fit each time trace to the phenomenological function [42]:

$$u(t) = 1 + [\theta(t - t_0)I_\infty(1 - \alpha e^{-(t-t_0)/\tau})] \circ g(w_0, t), \quad (1)$$

where $\theta(t)$ denotes the Heaviside step function, $g(w_0, t)$ is the cross-correlation of the pump and probe pulses and the symbol \circ indicates convolution. This allows us to extract three parameters: (i) the time constant of the transient decay, τ ; (ii) the SHG intensity at late times relative to the intensity before the pulse I_∞ ; and (iii) the fraction of I_∞ that is related to the dynamics associated with τ , α . The best-fit values for τ , I_∞ , and αI_∞ are plotted as a function of fluence in Fig. 3(b). We find that I_∞ decreases with increasing fluence until reaching a saturation $I_\infty^{\text{sat}} \approx -0.11$ at fluence $F_{\text{sat}} \approx 0.4 \text{ mJ/cm}^2$, while αI_∞ decreases from zero to roughly half of I_∞^{sat} near F_{sat} before increasing at high fluence. The time constant τ exhibits the most noteworthy behavior; it first increases by nearly an order of

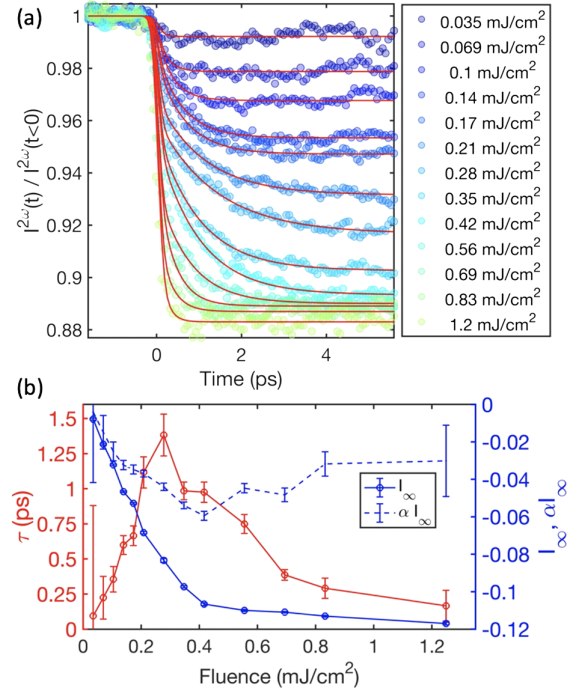


FIG. 3. (a) Time evolution of the normalized SHG intensity, $I^{2\omega} \propto |\chi_{baa}^{ED}|^2$, for varying pump fluences, measured at a nominal temperature of 4 K (laser heating raises the temperature). Fits to Eq. (1) are overlaid in red. (b) Best-fit values of I_∞ , αI_∞ , and τ plotted vs pump fluence. Error bars are 95% confidence intervals from the fitting procedure.

magnitude from $< 200 \text{ fs}$ to $\sim 1.4 \text{ ps}$, peaking near F_{sat} before decreasing to roughly 200 fs .

For fluences $F \gtrsim F_{\text{sat}}$, these measurements suggest that the sample has reverted to the high-temperature structure; the intensity jump observed as a function of temperature [Fig. 1(c)] is completely suppressed by the photoexciting laser pulse. However, the nature of the “intermediate” states, characterized by $0 < |I_\infty| < |I_\infty^{\text{sat}}|$ is not immediately obvious. There are two natural possible scenarios to attribute to these states. In the first scenario, the lattice parameters would change in a spatially uniform manner throughout the illuminated region and would take on a value between that of the low- and high-temperature equilibrium phases. Alternatively, the effect of the pulse could be spatially nonuniform and the intermediate states could consist of small regions in which the lattice parameters primarily take on either their low- or high-temperature equilibrium values.

For several reasons, including the discontinuous character of the equilibrium transition and the observation of structural inhomogeneity in the hysteresis region of Ti-substituted CRO [61,62], we expect *a priori* that the lattice parameters exhibit discontinuous changes. We show below that this scenario accounts for the experimental observations, most notably the nonmonotonic fluence dependence of the timescale τ [Fig. 3(b)].

To demonstrate that binary values of the lattice parameters can give rise to this behavior, we perform a bootstrap percolation simulation. The simulation consists of the following recipe [63]. (In the following, for ease of presentation, we refer only to the c -axis changes, but this is meant to represent the changes to all lattice parameters.) (1) An array of sites is defined that can take only a long or short c -axis lattice parameter, denoted L_c and S_c , respectively. Before $t = 0$ the system is initialized to possess only S_c sites, corresponding to the low-temperature insulating state. (2) At $t = 0$, a random subset of sites is switched to the L_c state to mimic the effect of the pump. The number of switched sites is assumed to be proportional to the incident pump fluence. (3) Each remaining S_c site then evolves according to the governing rule that if the number of nearest neighbor L_c sites *exceeds* a threshold value σ_{th} , the examined site switches from S_c to L_c . (4) Lastly, once converted to an L_c site, it is forbidden from reverting to an S_c one. These rules encompass the entire simulation, and it is run in discrete time steps until the system reaches quasiequilibrium where site switching no longer occurs. Imposition of the rule (4) is motivated by data showing that the recovery to the state with a globally contracted c axis occurs on much longer timescales [42]. Because we disallow L_c -to- S_c conversion, the model describes a manifestly nonequilibrium process characterized by a breakdown of detailed balance and a transition to an absorbing state. With this minimal model taking a single input parameter σ_{th} , we are able to capture the qualitative behavior of all three fitted parameters in our data.

In our implementation, the sample is modeled as a $40 \times 40 \times 40$ cubic array of sites. The fraction of sites that are excited at $t = 0$ is given by the fluence fraction parameter f , which is defined between 0 and 1, corresponding, respectively, to no pump pulse and to a pulse that excites all of the sites quasi-instantaneously. At each time step, the “strain” at each site σ is equal to the number of neighboring sites in the L_c state [42]. In the results of the simulation shown in Fig. 4, the threshold parameter σ_{th} is equal to three. To correlate the simulation to our data, we make the assumption that the change in $I^{2\omega}$ at each time step is proportional to the fraction of sites that have switched to the L_c state. This correspondence allows us to produce the simulated time traces in Fig. 4(a). Finally, we fit the simulated time traces to Eq. (1) [without the finite pulse width factor $g(w_0, t)$] to extract I_∞ , α , and τ as a function of the fluence fraction f [Fig. 4(b)] [42].

Figure 4 shows that this model reproduces all of the qualitative aspects of the SHG response. We emphasize that these simulations did not require fine-tuning to produce the desired results. Rather, we find that the nonmonotonic fluence dependences of τ and of α , with peaks near F_{sat} , are robust to changes of σ_{th} and to the inclusion of additional neighbor couplings, both when the simulation is confined to two dimensions and when the penetration depths of the

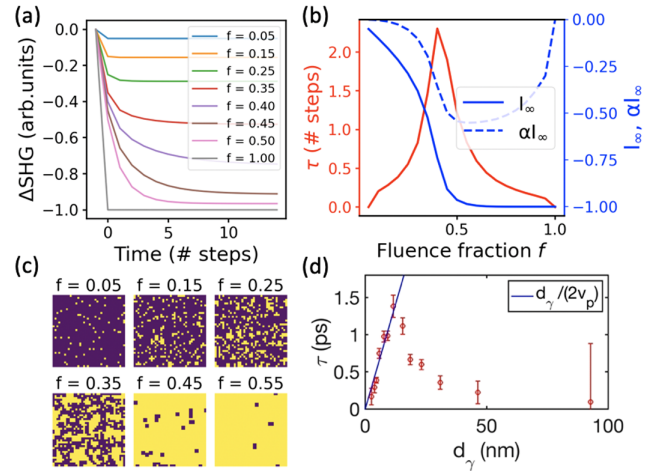


FIG. 4. (a) Simulated temporal evolution of SHG intensity for various fluence fractions f with strain threshold $\sigma_{\text{th}} = 3$. ΔSHG is determined from the fraction of sites in the L_c state. Time steps indicate iterations of the simulation. (When compared to the experiment, each time step corresponds to a few hundred femtoseconds.) (b) The parameters τ , I_∞ , and αI_∞ determined from the simulations plotted against the fluence fraction parameter f . (c) Examples of two-dimensional slices of the final system state for various fluence fractions f . $L_c(S_c)$ sites are depicted in yellow (purple). We estimate that each site corresponds to a region of the material with a length scale on the order of 1 nm [42]. (d) τ plotted versus the average distance between absorbed pump photons d_γ . The linear fit to the data in the high-fluence regime allows us to extract an approximate percolation speed v_p .

pump and probe pulses are taken into account. See Supplemental Material [42] for details of the simulations using alternate settings.

We are left with the following physical picture to explain the nonmonotonic behavior of the timescale τ . At low fluences, random isolated sites are photoexcited to the L_c state, but these sites cannot percolate very far; the S_c sites do not possess a sufficient number of L_c nearest neighbors to trigger a switching event. The observed transition time is therefore on the order of the exciting laser pulse in the experiment. As the fluence is increased, some sites that remained in the S_c state after the initial photoexcitation exceed the nearest neighbor strain threshold and turn into an L_c site. The L_c sites then start to percolate; switching events are able to trigger further switching events. Near the percolation threshold, where almost all the sites are switched, the transition time starts to lengthen considerably, mimicking critical slowing down [64]. At higher fluences, the number of sites that switch to the L_c state instantaneously is large and only a short time is needed to switch the remaining S_c sites. Within this framework, the peak in τ physically represents the maximum time it takes for the L_c site percolation to occur following the initial photoexcitation.

This physical picture also lends itself to a natural interpretation of the parameters I_∞ and α . In this scheme, I_∞ represents the total number of switched sites, including

both the quasi-instantaneous effects from photoexcitation and the subsequent percolation. On the other hand, α describes the fraction of sites that convert from S_c to L_c solely due to percolation, and its dynamics are associated with the timescale τ . The dip in αI_∞ with varying fluence thus indicates that the volume of the sample induced to become L_c through site-to-site spreading is largest at fluences near F_{sat} , in accordance to what would be expected near a percolation threshold [Fig. 4(b)]. The interpretation of these parameters allows us to understand the PIPT as a percolation phenomenon mediated by local interactions between neighboring sites.

A physical justification that the interactions are mediated by lattice strain is obtained by an estimate of the percolation speed v_p . We first convert the fluence to an average distance between absorbed pump photons d_γ [42]. For fluences $F > F_{\text{sat}}$, this quantity characterizes the length over which an average L_c region percolates. (This is not the case for $F < F_{\text{sat}}$ when S_c regions will persist between sites excited by photons.) We find that τ is linearly proportional to d_γ in this high-fluence (low d_γ) regime, indicating that the percolation speed is independent of fluence. Performing a linear fit, we extract a characteristic growth speed of ~ 4400 m/s [Fig. 4(d)]. Though the speed of sound has not been measured in $\text{Ca}_3\text{Ru}_2\text{O}_7$, this value is in accord with what would be expected if the growth of L_c clusters was given by ballistic strain propagation.

In summary, our study provides substantial evidence that the kinetics of the PIPT in $\text{Ca}_3\text{Ru}_2\text{O}_7$ proceeds through the percolation of nanoscale clusters which is mediated by lattice strain. Specifically, the transition dynamics are qualitatively captured by a model of bootstrap percolation. The simplicity of this model suggests that it may hold significant promise for understanding the dynamics of other PIPTs. Indeed, time-resolved measurements of the photo-induced transition in VO_2 [18,21,65,66] shows two time-scales of comparable duration to those observed in this work, which may also be described within a percolation theory. Our work paves the way toward understanding the effects of dynamic inhomogeneity on PIPTs and provides a general model that may be useful for investigating photo-excited materials more broadly.

We thank R. Schonmann for helpful discussions regarding the percolation model, M. Rasiah for help with the initial construction of the second harmonic generation setup, and S. Kivelson for helpful suggestions regarding the Landau theory calculation. Research at U.C.L.A. was supported by the U.S. Department of Energy (DOE), Office of Science, Office of Basic Energy Sciences under Award No. DE-SC0023017 (experiment and simulations). Work at UC Boulder was supported by the National Science Foundation via Grant No. DMR 2204811 (materials synthesis). A. Z. acknowledges support by the Miller Institute for Basic Research in Science. A. K., R. A., and C. J. A.

acknowledge the REU program through STROBE: a National Science Foundation Science and Technology Center under Grant No. DMR-1548924.

*tcarbin@g.ucla.edu

†anshulkogar@physics.ucla.edu

- [1] L. Stojchevska, I. Vaskivskiy, T. Mertelj, P. Kusar, D. Svetin, S. Brazovskii, and D. Mihailovic, *Science* **344**, 177 (2014).
- [2] J. Zhang, X. Tan, M. Liu, S. W. Teitelbaum, K. W. Post, F. Jin, K. A. Nelson, D. N. Basov, W. Wu, and R. D. Averitt, *Nat. Mater.* **15**, 956 (2016).
- [3] M. Mitrano, A. Cantaluppi, D. Nicoletti, S. Kaiser, A. Perucchi, S. Lupi, P. Di Pietro, D. Pontiroli, M. Riccò, S. R. Clark, D. Jaksch, and A. Cavalleri, *Nature (London)* **530**, 461 (2016).
- [4] D. Fausti, R. I. Tobey, N. Dean, S. Kaiser, A. Dienst, M. C. Hoffmann, S. Pyon, T. Takayama, H. Takagi, and A. Cavalleri, *Science* **331**, 189 (2011).
- [5] A. Kogar *et al.*, *Nat. Phys.* **16**, 159 (2020).
- [6] J. W. McIver, B. Schulte, F.-U. Stein, T. Matsuyama, G. Jotzu, G. Meier, and A. Cavalleri, *Nat. Phys.* **16**, 38 (2020).
- [7] D. Perez-Salinas, A. S. Johnson, D. Prabhakaran, and S. Wall, *Nat. Commun.* **13** (2022).
- [8] D. Mihailovic and V. V. Kabanov, Dynamic inhomogeneity, pairing and superconductivity in cuprates, in *Superconductivity in Complex Systems*, edited by K. A. Müller and A. Bussmann-Holder (Springer, Berlin, Heidelberg, 2005), pp. 331–364.
- [9] E. Abreu, S. Wang, J. G. Ramírez, M. Liu, J. Zhang, K. Geng, I. K. Schuller, and R. D. Averitt, *Phys. Rev. B* **92**, 085130 (2015).
- [10] W. S. Lee *et al.*, *Nat. Commun.* **3**, 838 (2012).
- [11] E. Abreu, D. Meyers, V. K. Thorsmølle, J. Zhang, X. Liu, K. Geng, J. Chakhalian, and R. D. Averitt, *Nano Lett.* **20**, 7422 (2020).
- [12] S. Wall, S. Yang, M. Kozina, T. Katayama, T. Henighan, M. Trigo, O. Delaire, L. A. Boatner, D. A. Reis, T. A. Miller, M. Jiang, J. M. Glowia, M. Chollet, and L. Vidas, *Science* **362**, 572 (2018).
- [13] A. J. Sternbach, F. L. Ruta, Y. Shi, T. Slusar, J. Schalch, G. Duan, A. S. McLeod, X. Zhang, M. Liu, A. J. Millis, H.-T. Kim, L.-Q. Chen, R. D. Averitt, and D. N. Basov, *Nano Lett.* **21**, 9052 (2021).
- [14] A. S. Johnson, D. Perez-Salinas, K. M. Siddiqui *et al.*, *Nat. Phys.* **19**, 215 (2022).
- [15] B. T. O’Callahan, A. C. Jones, J. Hyung Park, D. H. Cobden, J. M. Atkin, and M. B. Raschke, *Nat. Commun.* **6**, 6849 (2015).
- [16] S. A. Dönges, O. Khatib, B. T. O’Callahan, J. M. Atkin, J. H. Park, D. Cobden, and M. B. Raschke, *Nano Lett.* **16**, 3029 (2016).
- [17] D. J. Hilton, R. P. Prasankumar, S. Fourmaux, A. Cavalleri, D. Brassard, M. A. El Khakani, J. C. Kieffer, A. J. Taylor, and R. D. Averitt, *Phys. Rev. Lett.* **99**, 226401 (2007).
- [18] M. R. Otto, L. P. R. de Cotret, D. A. Valverde-Chavez, K. L. Tiwari, N. Émond, M. Chaker, D. G. Cooke, and B. J. Siwick, *Proc. Natl. Acad. Sci. U.S.A.* **116**, 450 (2019).

- [19] S. E. Madaras, J. A. Creeden, D. J. Lahneman, A. Harbick, D. B. Beringer, M. M. Qazilbash, I. Novikova, and R. A. Lukaszew, *Opt. Mater. Express* **10**, 1393 (2020).
- [20] M. Rodriguez-Vega, M. T. Simons, E. Radue, S. Kittiwatanakul, J. Lu, S. A. Wolf, R. A. Lukaszew, I. Novikova, and E. Rossi, *Phys. Rev. B* **92**, 115420 (2015).
- [21] T. L. Cocker, L. V. Titova, S. Fourmaux, G. Holloway, H.-C. Bandulet, D. Brassard, J.-C. Kieffer, M. A. El Khakani, and F. A. Hegmann, *Phys. Rev. B* **85**, 155120 (2012).
- [22] K. Haupt, M. Eichberger, N. Erasmus, A. Rohwer, J. Demsar, K. Rossnagel, and H. Schwoerer, *Phys. Rev. Lett.* **116**, 016402 (2016).
- [23] C. Laulhé *et al.*, *Phys. Rev. Lett.* **118**, 247401 (2017).
- [24] T. Danz, T. Domröse, and C. Ropers, *Science* **371**, 371 (2021).
- [25] A. Zong, A. Kogar, Y.-Q. Bie, T. Rohwer, C. Lee, E. Baldini, E. Ergeçen, M. B. Yilmaz, B. Freelon, E. J. Sie, H. Zhou, J. Straquadine, P. Walmsley, P. E. Dolgirev, A. V. Rozhkov, I. R. Fisher, P. Jarillo-Herrero, B. V. Fine, and N. Gedik, *Nat. Phys.* **15**, 27 (2019).
- [26] D. Cho, S. Cheon, K.-S. Kim, S.-H. Lee, Y.-H. Cho, S.-W. Cheong, and H. W. Yeom, *Nat. Commun.* **7**, 10453 (2016).
- [27] L. Ma, C. Ye, Y. Yu, X. Lu, X. Niu, S. Kim, D. Feng, D. Tománek, Y.-W. Son, X. Chen, and Y. Zhang, *Nat. Commun.* **7**, 10956 (2016).
- [28] A. S. McLeod, J. Zhang, M. Q. Gu, F. Jin, G. Zhang, K. W. Post, X. G. Zhao, A. J. Millis, W. B. Wu, J. M. Rondinelli, R. D. Averitt, and D. N. Basov, *Nat. Mater.* **19**, 397 (2020).
- [29] Y. Yoshida, S.-I. Ikeda, H. Matsuhata, N. Shirakawa, C. H. Lee, and S. Katano, *Phys. Rev. B* **72**, 054412 (2005).
- [30] W. Bao, Z. Q. Mao, Z. Qu, and J. W. Lynn, *Phys. Rev. Lett.* **100**, 247203 (2008).
- [31] I. Marković, M. D. Watson, O. J. Clark, F. Mazzola, E. A. Morales, C. A. Hooley, H. Rosner, C. M. Polley, T. Balasubramanian, S. Mukherjee, N. Kikugawa, D. A. Sokolov, A. P. Mackenzie, and P. D. C. King, *Proc. Natl. Acad. Sci. U.S.A.* **117**, 15524 (2020).
- [32] M. Horio *et al.*, *npj Quantum Mater.* **6**, 29 (2021).
- [33] F. Baumberger, N. J. C. Ingle, N. Kikugawa, M. A. Hossain, W. Meevasana, R. S. Perry, K. M. Shen, D. H. Lu, A. Damascelli, A. Rost, A. P. Mackenzie, Z. Hussain, and Z.-X. Shen, *Phys. Rev. Lett.* **96**, 107601 (2006).
- [34] G. Cao, S. McCall, J. E. Crow, and R. P. Guertin, *Phys. Rev. Lett.* **78**, 1751 (1997).
- [35] B. Bohnenbuck, I. Zegkinoglou, J. Stremper, C. Schüßler-Langeheine, C. S. Nelson, P. Leininger, H.-H. Wu, E. Schierle, J. C. Lang, G. Srajer, S. I. Ikeda, Y. Yoshida, K. Iwata, S. Katano, N. Kikugawa, and B. Keimer, *Phys. Rev. B* **77**, 224412 (2008).
- [36] J. F. Karpus, R. Gupta, H. Barath, S. L. Cooper, and G. Cao, *Phys. Rev. Lett.* **93**, 167205 (2004).
- [37] J. Peng, M. Q. Gu, X. M. Gu, G. T. Zhou, X. Y. Gao, J. Y. Liu, W. F. Xu, G. Q. Liu, X. Ke, L. Zhang, H. Han, Z. Qu, D. W. Fu, H. L. Cai, F. M. Zhang, Z. Q. Mao, and X. S. Wu, *Phys. Rev. B* **96**, 205105 (2017).
- [38] F. Lechermann, Q. Han, and A. J. Millis, *Phys. Rev. Res.* **2**, 033490 (2020).
- [39] D. Puggioni, M. Horio, J. Chang, and J. M. Rondinelli, *Phys. Rev. Res.* **2**, 023141 (2020).
- [40] M. Fiebig, V. V. Pavlov, and R. V. Pisarev, *J. Opt. Soc. Am. B* **1**, 96 (2005).
- [41] J. Bertinshaw, M. Krautloher, H. Suzuki, H. Takahashi, A. Ivanov, H. Yavaş, B. J. Kim, H. Gretarsson, and B. Keimer, *Phys. Rev. B* **103**, 085108 (2021).
- [42] See Supplemental Material at <http://link.aps.org/supplemental/10.1103/PhysRevLett.130.186902> for more data analysis, theoretical calculations, and simulation results, which includes Refs. [43–57].
- [43] J. S. Lee, S. J. Moon, B. J. Yang, J. Yu, U. Schade, Y. Yoshida, S.-I. Ikeda, and T. W. Noh, *Phys. Rev. Lett.* **98**, 097403 (2007).
- [44] R. H. Schonmann, *Ann. Probab.* **20**, 174 (1992).
- [45] J. Balogh, B. Bollobás, and R. Morris, *Ann. Probab.* **37**, 1329 (2009).
- [46] J. Balogh, B. Bollobás, H. Duminil-Copin, and R. Morris, *Trans. Am. Math. Soc.* **364**, 2667 (2012).
- [47] A. E. Holroyd, *Probab. Theory Related Fields* **125**, 195 (2003).
- [48] V. Varadarajan, S. Chikara, V. Durairaj, X. Lin, G. Cao, and J. Brill, *Solid State Commun.* **141**, 402 (2007).
- [49] A. Y. Kuznetsov, V. P. Dmitriev, O. I. Bandilet, and H.-P. Weber, *Phys. Rev. B* **68**, 064109 (2003).
- [50] G. Azzolina, R. Berton, C. Ecolivet, H. Tokoro, S.-i. Ohkoshi, and E. Collet, *Phys. Rev. B* **102**, 134104 (2020).
- [51] M. C. Shapiro, P. Hlobil, A. T. Hristov, A. V. Maharaj, and I. R. Fisher, *Phys. Rev. B* **92**, 235147 (2015).
- [52] P. S. Pershan, *Phys. Rev.* **130**, 919 (1963).
- [53] D. Sa, R. Valentí, and C. Gros, *Eur. Phys. J. B* **14**, 301 (2000).
- [54] N. A. Benedek and C. J. Fennie, *Phys. Rev. Lett.* **106**, 107204 (2011).
- [55] A. B. Harris, *Phys. Rev. B* **84**, 064116 (2011).
- [56] N. A. Benedek, A. T. Mulder, and C. J. Fennie, *J. Solid State Chem.* **195**, 11 (2012).
- [57] E. A. Nowadnick and C. J. Fennie, *Phys. Rev. B* **94**, 104105 (2016).
- [58] S. Lei, S. Chikara, D. Puggioni, J. Peng, M. Zhu, M. Gu, W. Zhao, Y. Wang, Y. Yuan, H. Akamatsu, M. H. W. Chan, X. Ke, Z. Mao, J. M. Rondinelli, M. Jaime, J. Singleton, F. Weickert, V. S. Zapf, and V. Gopalan, *Phys. Rev. B* **99**, 224411 (2019).
- [59] X. Ke, J. Peng, W. Tian, T. Hong, M. Zhu, and Z. Q. Mao, *Phys. Rev. B* **89**, 220407(R) (2014).
- [60] S. Lei, M. Gu, D. Puggioni, G. Stone, J. Peng, J. Ge, Y. Wang, B. Wang, Y. Yuan, K. Wang, Z. Mao, J. M. Rondinelli, and V. Gopalan, *Nano Lett.* **18**, 3088 (2018).
- [61] A. S. McLeod, A. Wieteska, G. Chiriaco, B. Foutty, Y. Wang, Y. Yuan, F. Xue, V. Gopalan, L. Q. Chen, Z. Q. Mao, A. J. Millis, A. N. Pasupathy, and D. N. Basov, *npj Quantum Mater.* **6**, 46 (2021).
- [62] K. S. Rabinovich, A. N. Yaresko, R. D. Dawson, M. J. Krautloher, Y. L. Mathis, B. Keimer, and A. V. Boris, [arXiv:2206.05005](https://arxiv.org/abs/2206.05005).
- [63] J. Adler, *Physica (Amsterdam)* **171A**, 453 (1991).
- [64] A. Zong *et al.*, *Phys. Rev. Lett.* **123**, 097601 (2019).
- [65] S. Wall, L. Foglia, D. Wegkamp, K. Appavoo, J. Nag, R. F. Haglund, J. Stähler, and M. Wolf, *Phys. Rev. B* **87**, 115126 (2013).
- [66] H.-W. Liu, W.-H. Liu, Z.-J. Suo, Z. Wang, J.-W. Luo, S.-S. Li, and L.-W. Wang, *Proc. Natl. Acad. Sci. U.S.A.* **119**, e2122534119 (2022).